IN-CLINIC CALIBRATION OF A KERMA-AREA PRODUCT METER AT DIFFERENT RADIATION QUALITIES FOR THE ASSESSMENT OF SKIN DOSES INCURRED DURING INTERVENTIONAL FLUOROSCOPIC PROCEDURES

By

DAVID BORREGO

A THESIS PRESENTED TO THE GRADUATE SCHOOL
OF THE UNIVERSITY OF FLORIDA IN PARTIAL FULFILLMENT
OF THE REQUIREMENTS FOR THE DEGREE OF
MASTER OF SCIENCE

UNIVERSITY OF FLORIDA

2012

To my mother and sister for their steadfast support in my endeavors and their display of unconditional love

ACKNOWLEDGMENTS

Sincere thanks to my advisor and mentor, Dr. Wesley Bolch, for his guidance and encouragement through the past couple years. I thank Dr. Daniel Siragusa for allowing the use of his equipment and valuable feedback through the course of the project. I thank Dr. Kevin Johnson for his hard work in obtaining IRB approval and overall know-how with working on the PACS system and extracting RDSR. Thank you to Dr. David Hintenlang and Dr. David Gilland for their input, guidance, and serving as my instructors throughout my graduate school career. Thank you, Dr. Perry Johnson for laying down the groundwork.

TABLE OF CONTENTS

LIST OF TABLES

LIST OF FIGURES

LIST OF ABBREVIATIONS

ALRADS	Advanced Laboratory for Radiation and Dosimetry Studies
CD	Cumulative dose
DAP	Dose area product
FDA	Food and Drug Administration
ICRP	International Commission on Radiological Protection
IEC	International Electrotechnical Commission
IR	Interventional Radiology
KAP	Kerma area product
NCRP	National Council on Radiation Protection
PSD	Peak skin dose
VIR	Vascular Interventional Radiology

Abstract of Thesis Presented to the Graduate School
of the University of Florida in Partial Fulfillment of the
Requirements for the Degree of Master of Science

IN-CLINIC CALIBRATION OF A KERMA-AREA PRODUCT METER AT DIFFERENT RADIATION QUALITIES FOR THE ASSESSMENT OF SKIN DOSES INCURRED DURING INTERVENTIONAL FLUOROSCOPIC PROCEDURES

By

David Borrego

December 2012

Chair: Wesley Bolch
Major: Biomedical Engineering

The growing use and increasing complexity of interventional fluoroscopic procedures has raised public health concerns regarding radiation exposure to both the patient's skin and internal radiosensitive organs. Current dosimetry options available to clinicians and physicians fail to account for the dynamic nature of fluoroscopic procedures and anthropometric differences in-patient size. The University of Florida skin dose mapping and organ software overcome these challenges my making use of the Radiation Dose Structured Report and the UF hybrid adult patient-dependent series of computational phantoms; however, it still relies on measurements from the kerma-area product meter. The kerma-area product meter is only accurate to within ±35% to account for uncertainties in determining patient skin dose. In order to address the inherent uncertainty introduced into the skin dose software from the ionization chamber, calibration coefficients were introduced. The calibration coefficients show strong energy dependence and can be predicted with knowledge of the tube voltage and amount of filtration material in the beam. The skin dose mapping software is able to cull for those

variables, calculate the calibration coefficient, and finally apply the corrections in its calculation of dose. Overall, this study was able to show that many of the clinical challenges encountered in dose reconstructions may be overcome to eventually provide physicians with accurate real-time skin dose information to better help them manage patient risk.

CHAPTER 1
INTRODUCTION

Interventional Fluoroscopy

Interventional fluoroscopic procedures use ionizing radiation to visualize human anatomy and physiology in real time. These images aid physicians in guiding surgical instruments though blood vessels and other pathways in the body to the site of interest. This radiologic technique was born from diagnostic angiography and its development was lead by Charles Dotter in the early 1960s. Since then, interventional fluoroscopy has expanded greatly in many different medical fields owing to its advantages over surgical procedures and improved patient care. Interventional fluoroscopic procedures have reduced the need for more invasive surgical procedures reducing the morbidity and mortality of numerous diseases.[1] In contrast to invasive surgical procedures, interventional radiology requires only a small incision to be made for the introduction of instruments into the body—greatly reducing the risks of infections, complications, and recovery times.

Need for Comprehensive Dosimetry

The growing use and increasing complexity of interventional fluoroscopic procedures, however, has resulted in public health concerns regarding both deterministic risks of skin damage and, particularly for younger patients, stochastic cancer risks to irradiated tissues and radiosensitive organs. Tracking and documenting patient-specific skin and internal organ dose has been specifically identified for interventional fluoroscopy where extended irradiation times, multiple projections, and repeat procedures can lead to some of the largest doses encountered in both radiology

and cardiology. Furthermore, in-procedure knowledge of localized skin doses can be of significant clinical importance to help physicians better manage patient risk.

The effective dose per capita within the United States has risen by a factor of six from 1980 to 2006 primarily driven by the increased use of ionizing radiation in diagnostic imaging. Fluoroscopically guided procedures have doubled in frequency from 1996 to 2000, and as the number of procedures per capita has increased so has their complexity, with many requiring longer procedure times.[2] Such an increase in the use of ionizing radiation has prompted strong recommendations from the scientific, medical, and legislative communities to encourage patient-specific tracking of medical doses for inclusion in medical records. The state of California has already led the way by passing SB-1237, which requires radiation dose from computed tomography (CT) to be included in patient medical records. The Center for Devices and Radiological Health (CDRH) of the US FDA released in February 2010 a comprehensive initiative to "reduce unnecessary radiation exposures from medical imaging"—specifically addressing doses incurred during fluoroscopically guided interventions.[3] The effective dose estimated for interventional procedures ranges from 10-300 mSv, well above those for radiographic images, CT, and nuclear medicine examinations. In February 2011, the National Council on Radiation Protection and Measurement (NCRP) released its Report No. 168. This comprehensive document includes 31 recommendations, ten of which relate to patient dose monitoring and documentation.[4] The significance of these recommendations highlights one of the primary concerns of the interventional physician—the management of radiological risk and specifically the management of radiation induced skin injury.

The effects of radiation damage to the skin can range from transient erythema and epilation to severe dermal atrophy, induration, and ulceration with the latter often-requiring surgical intervention.[5] Considerable efforts have been devoted toward the prevention of such injuries through intensive training of residents, the development of dose reducing imaging systems and an overall increase in physician awareness. While these efforts have reduced the incidence of injury, any damage that does occur is almost always unanticipated, yet in many cases is avoidable had prior knowledge of peak skin dose and approaching thresholds been available. Due to the current lack of automated skin dose monitoring, this type of information is being denied to the physician who must then rely on indirect dose metrics along with their clinical experience to manage patient risk.[6] Additionally, The Joint Commission has specifically identified prolonged fluoroscopy use with a cumulative peak skin doses > 15 Gy to a single field as a sentinel event requiring root cause analysis and a comprehensive response.[7] A root cause analysis places a huge burden on clinical staff to reconstruct skin dose when a sentinel event is thought to have occurred. The lack of direct and real-time automated skin dose monitoring system in the clinic thus limits both the quality of patient care and the efficiency of the interventional unit for designing better safeguards.

Limitations in IR dosimetry

To address public health concerns and those expressed by the scientific community, a variety of dose tracking systems have been developed to indirectly or directly quantify the cumulative organ and local skin dose in real-time or as a post procedure report. The methods include the use of total fluoroscopy time, kerma-area product, cumulative air kerma at the reference point, and the use of both point dosimeter or film dosimetry.

Fluoroscopy timers are the simplest and only dose metric employed by most interventional fluoroscopic units for clinical radiation management. Despite being the most commonly used dose metric, it is also arguably the most inadequate estimator of dose. The timer works by emitting an audible alert every five minutes of cumulative fluoroscopic time. This metric completely disregards important dose parameters such as radiation quality, fluoroscopic dose rate, image acquisitions and their contributions to dose, beam's entrance port, and anthropometric variations in patient size.[8]

The air kerma-area product, more commonly known as the dose area product, is defined as the air-kerma integrated over the beams area. This metric may be directly measured with the use of an ionization chamber installed in the fluoroscopic unit or through tabulated parameters of irradiation techniques. The cumulative kerma-area product (or KAP) is a better indicator of maximum skin dose than total fluoroscopy time; however, the KAP fails to account for field non-uniformity effects and the field size.[8,9] An extension of the KAP is the cumulative air kerma at the reference point, ($K_{a,r}$), which displays the reference air-kerma defined relative to the isocenter of the imaging system, as proposed by The International Electrotechnical Commission's standard. Both the KAP and $K_{a,r}$ fail to account for the dynamic nature of fluoroscopically guided procedures and have allowable uncertainties of up to ±35%.[8]

Thermoluminescent dosimeters (TLD), optically stimulated luminescence (OSL) chips, and diodes as point dosimeters can provide a direct measure of dose under proper calibration and when applied prior to the procedure on the patient's skin. Both TLDs and OSLs fail to provide real-time dosimetry but may be used for retrospective

analysis. Diodes can provide real-time dose feedback; however, knowledge of correct placement to measure the peak skin dose is required and is seldom a clinical possibility.

Film dosimetry provides the advantage of not having to precisely estimate where the occurrence of the peak skin dose will manifest itself; rather only a general idea of location is needed. Dosimetry with the use of film can provide great spatial knowledge with regards to the dose distribution on the patient's skin; however, most films only have a working range up to 2 Gy. The films working sensitivity leaves much to be desired for the complex interventional fluoroscopic procedures where the dose commonly exceeds the upper detection limits of the film.

University of Florida skin dose mapping software

In contrast to the previously mentioned dosimetry systems, the University of Florida's skin dose mapping software for interventional fluoroscopy is unique by taking advantage of two innovations that increase the prospects for accurate automated dose monitoring. First, the software system makes use of the UF hybrid adult patient-dependent series of computational phantoms. These models represent the best choice for medical dosimetry because they rely on anthropometric measurements to match the characteristics of individual patients.[10] Secondly, the introduction of the Radiation Dose Structured Report (RDSR) allows the software to address directly the dynamic nature of interventional procedures.

Anthropometric phantoms. The UF Advanced Laboratory for Radiation and Dosimetry Studies (ALRADS) has developed hybrid phantoms and pioneered the methods for patient-phantom matching, whereby individuals are computationally matched to a similar hybrid phantom based on anthropometric parameters. For skin dose calculations, the primary factor affecting dose is the calculation of the source-to-

skin distance; therefore, even a slight change in the patient's outer body contour can lead to different estimations of peak skin dose. By correctly matching a patient to a phantom that is best representative of the individuals' body morphometry, the accuracy of skin dose estimates is greatly improved.[6]

Radiation dose structured report. For accurate dose reconstruction, a wealth of irradiation parameters are needed. Included in these conditions are exposure parameters (kVp, mAs, filtration material, filtration thickness, and KAP/$K_{a,r}$) and geometry factors (source-to-skin distance, field size, field position, rotation, angulation, and table location). The challenge presented in fluoroscopy is that the irradiation conditions are not typically standardized and change often during a given fluoroscopic procedure. There is the principal need for a system that monitors the irradiation conditions and produces an automated report, preferably in real- or near real-time. In response to this pressing need for standardization, The DICOM Committee published Supplement 94 to the DICOM standard. This update provided a framework for dose reporting by creating the RDSR. The RDSR records all pertinent exposure conditions and geometry factors needed for a dose reconstruction, save field size. Furthermore, the RDSR report stands as an independent DICOM object that is updated at the completion of each irradiation event during a fluoroscopic procedure.

The application of phantom-patient matching through the use of patient-dependant hybrid phantoms provides one solution for a two-part problem. The RDSR provides a framework to overcome the second challenge faced in dose reconstruction algorithms and that is the dynamic nature of interventional procedures. While the use of hybrid patient-dependent phantoms will increase the accuracy of current dosimetry

methods, the development and recent release of the RDSR will make them practical for the clinic.

Algorithm. The skin dose mapping software is written in PYTHON, an open source scientific programming language that allows for a robust graphical user interface and 3-Dimensional visualization techniques. The module Pydicom, a DICOM compatible reader for PYTHON, is used to extract geometric information and dose parameters found within the RDSR and populates a 2-Dimensonal array structure where each row is filled with the parameters corresponding to a single irradiation event. The information extracted from the RDSR is transformed into peak skin dose with the dose-mapping algorithm. This algorithm is then able to incorporate a variety of different phantom types to account for individual variations in patient body morphometry. The only requirement is that the phantom be voxelized prior to use. The voxelization of the phantom allows for the 3-Dimensonal localization of the phantom's skin as a set of x, y, z coordinates. The phantom coordinate system is then aligned with that of the Siemens Artis Zee system installed within the Department of Radiology at Shands Jacksonville Medical Center. Assuming a supine orientation with the tube located beneath the table, the posterior skin of the phantom rests at the tube isocenter. The position of the isocenter in relation to the head of the table is predetermined. The position of the patient's head in relation to the table is then used to locate the phantom longitudinally. The patient is assumed to lie in the middle of the table and a correction can be applied for any lateral displacement. Any shifts in table height, latitudinal, and longitudinal positions as identified by the RDSR are applied to the phantom. The primary and secondary angles are then used in

correspondence with the source-to-isocenter distance to determine the xyz location of the source relative to the phantom.

Unit vectors are then calculated from the origin, tube location, and in the direction of each xyz skin location. These unit vectors are then separated based on their position either inside or outside the irradiation filed. To differentiate between skin locations on the entrance and exit sides of the phantom, the source-to-skin distance for each location is determined to be within the beam is compared with the minimum source-to-skin distance. The program then rejects all unit vectors outside the irradiation projection and all non-entrance-side skin locations.

The dose is then calculated for each skin-affected area according to Equation 1.

$$Dose_{Skin} = K_{a,r} * \frac{d_{ref}^{2}}{d_{skin}^{2}} * BF * \left(\frac{\mu_{en}}{\rho}\right)_{air}^{skin} * e^{-\mu t} \quad (1)$$

The backscatter factor, BF, is selected from ICRU Report 74, the ratio of mass energy absorption coefficients for skin to air, $(\mu_{en}/\rho)_{skin}/(\mu_{en}/\rho)_{air}$ is determined from the NIST Physical Reference Data Library, and $e^{-\mu t}$ represents table attenuation. The peak skin dose is then calculated as the maximum of these doses after the dose from each irradiation event has been summed at each skin location.[6]

Kerma-Area Product Meter

As previously indicated, current dosimetry techniques in interventional radiology fail to account for the dynamic nature of these procedures and anthropometric variation in the population. The University of Florida skin dose mapping software addresses both these issues; however, it still relies on measurements from the KAP and $K_{a,r}$. Both the KAP and $K_{a,r}$ are measured with the use of a plane-parallel transmission ionization chamber which need only be accurate to ±35%.[8] The tolerance is allowed to be broad in

order to account for uncertainties in determining patient skin dose and variation in tissue biological response to dose. In order to address the inherent uncertainty introduced into the skin dose software from the ionization chamber, calibration coefficients are introduced.

The purpose of this study was to first develop a method for an in-clinic calibration of the Siemens Artis Zee kerma-area product meter. The calibration coefficient would need to take into account the strong dependence of the kerma-area product meter on the energy spectrum of the x-ray beam. Furthermore, issues have been raised over fluoroscopic units not reporting the true reading from the kerma-area product meter but rather a convoluted reading accounting for tube positioning and irradiation conditions. These proprietary algorithms needed to be investigated before a successful calibration could be achieved. Secondly, based on the meters interdependence of irradiation parameters, this study developed an algorithm that would be able to calculate the calibration coefficient for each irradiation event with the use of the RDSR and apply the correction factors to the skin dose mapping software.

CHAPTER 2
MATERIALS AND METHODS

Site and Materials

The Division of Vascular and Interventional Radiology at Shands Jacksonville was selected for the in-clinic calibration of a KAP meter. This facility is equipped a Siemens Medical Solutions Artis Zee bi-plane angiography system, Figure 2-1, which includes software for the generation of RDSR. This facility performs the full range of peripheral vascular interventions, as well as non-vascular interventional procedures – performing approximately 14,000 procedures each year. The Siemens Artis Zee is equipped with the DIAMENTOR M4-KDK DAP/Dose Meter featuring a transmission ion chamber that can measure air kerma, air kerma rate, and air kerma - area product simultaneously during radiographic and fluoroscopic procedures. Table 2-1 list the specifications of the KAP meter installed. To calibrate the KAP meter in the Siemens Artis Zee a Radcal 10x6-6 chamber, ion chamber digitizer 9660A, and Accu-Dose 2186 dosimeter system was used. The ionization chamber was selected for its relative flat energy response over the beam quality range of interest and dose rate sensitivity. A summary of the detectors specifications can be found in Table 2-2.

Calibration Set Up

The calibration coefficients of the KAP meter were measured with the use of the RADCAL ionization chamber placed at isocenter with the axis of the cylindrical chamber parallel to the axis of rotation for the C-arm. The chamber was held free in air with the use of a stand and a minimum clearance of 10 cm was provided between the chamber and tabletop. The position of the chamber may be verified by rotating the C-arm about the axis of rotation while acquiring images. If the chamber is at isocenter the image of

the chamber will translate but no rotation should be visible. The system is then set at maximum SID with the radiation field collimated so that un-irradiated margins are seen on all sides of the field and C-arm at 90^{o}, see Figure 2-2. With no wedges in place, an image of the ionization chamber is acquired under set up conditions to determine the radiation field size. Before performing the remaining measurements the detector array was removed and replaced with a lead insert to protect the integrity of the system form unnecessary radiation. The Siemens Artis Zee system is then set in service mode and the chamber is irradiated under the desired irradiation qualities. Alternatively, if service mode is unavailable, loading phantoms may be used to achieve the desired radiation qualities. The reference value for the kerma-area product (KAP_{ref}) was calculated as a product of the measured air kerma, $k_{a,r}$, at isocenter of the x-ray beam and the field area, A, at isocenter, Equation 2.

$$KAP_{ref} = K_{a,r} * A \tag{2}$$

The calibration coefficient, β, was taken as the quotient of the reference value and the KAP meter reading.

Determination of Calibration Coefficients

The KAP meter for the Siemens Artis Zee machine was calibrated for radiation incident on the chamber using x-ray tube voltages from 40-120 kVp and at 5 different tube filtrations of 0.1, 0.2, 0.3, 0.6, and 0.9 mm of Cu and also at tube voltages with no filtration. The effects of tube current and pulse width were also observed at high mAs combinations to insure that the KAP meter was not being saturated. These measurements were repeated at one-month intervals for four months to verify the reproducibility of the Siemens Artis Zee machine. One-way ANOVA analysis was

performed on these data to quantify the relationship between the calibration coefficients and how it relates to tube voltage, tube current, or filtration.

Implementation of Calibration Coefficients into Skin Dose Mapping Software and Testing

Calibration coefficient curves were developed as a function of tube voltage for each filtration and embedded into the skin dose mapping software. The algorithm in the skin dose mapping software was then modified to retrieve tube voltage and filtration information from the RDSR and calculates a calibration coefficient for each irradiation event. The calibration coefficient is then applied to correct the calculated skin doses.

The changes made to the skin dose mapping software where tested on RDSR from ten patients that were marked with relatively high cumulative reference air kerma values (see Table 2-4). The RDSR were obtained through an IRB protocol with Shands-Jacksonville Hospital from The Division of Vascular and Interventional Radiology. Procedure information along with patient height and weight were also obtained under this IRB protocol. The patient height and weight information was used to select patient-dependant hybrid phantoms from the UF Adult Hybrid Computational Phantom Series.

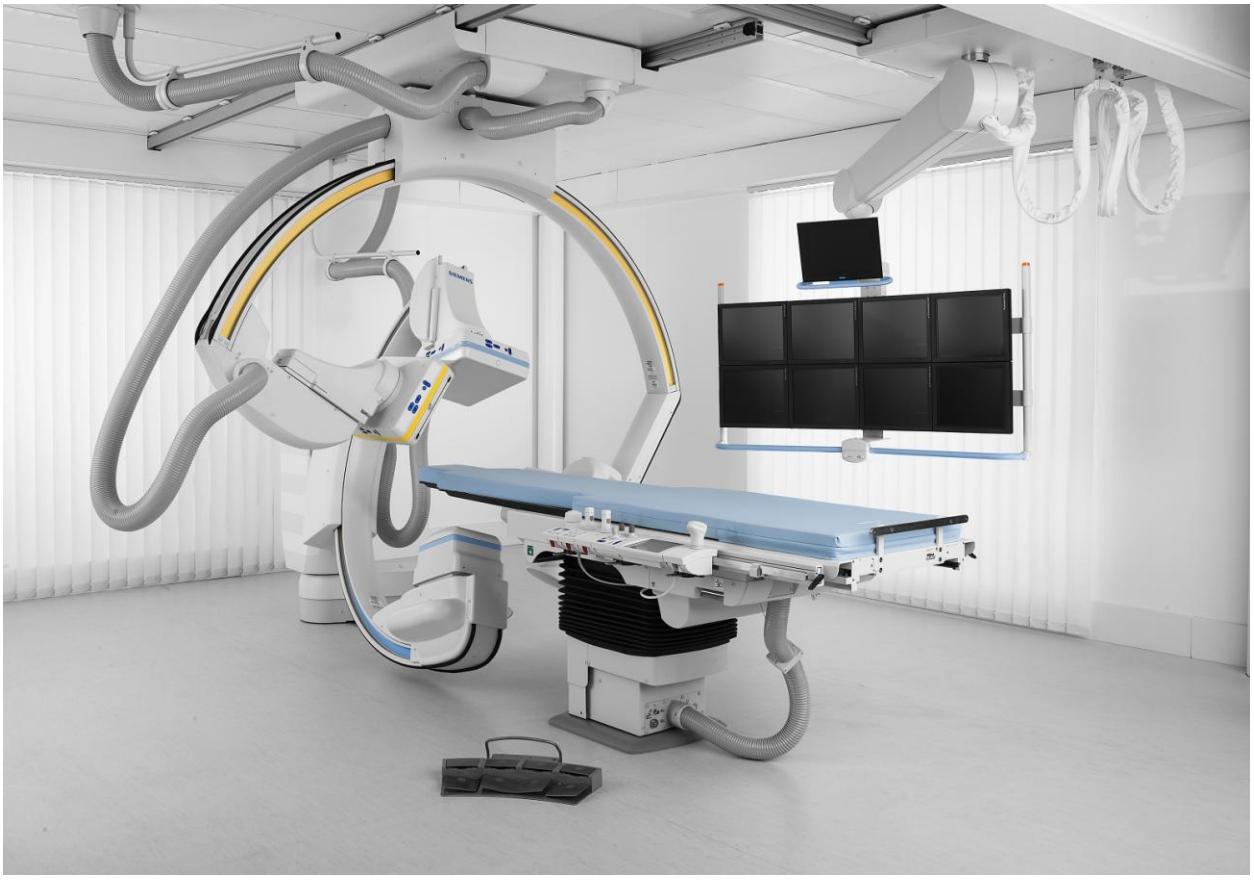

Figure 2-1. The Siemens Medical Solutions Artis Zee angiographic bi-plane system. (Photo courtesy of Siemens http://www.medical.siemens.com. Last accessed October, 2012).

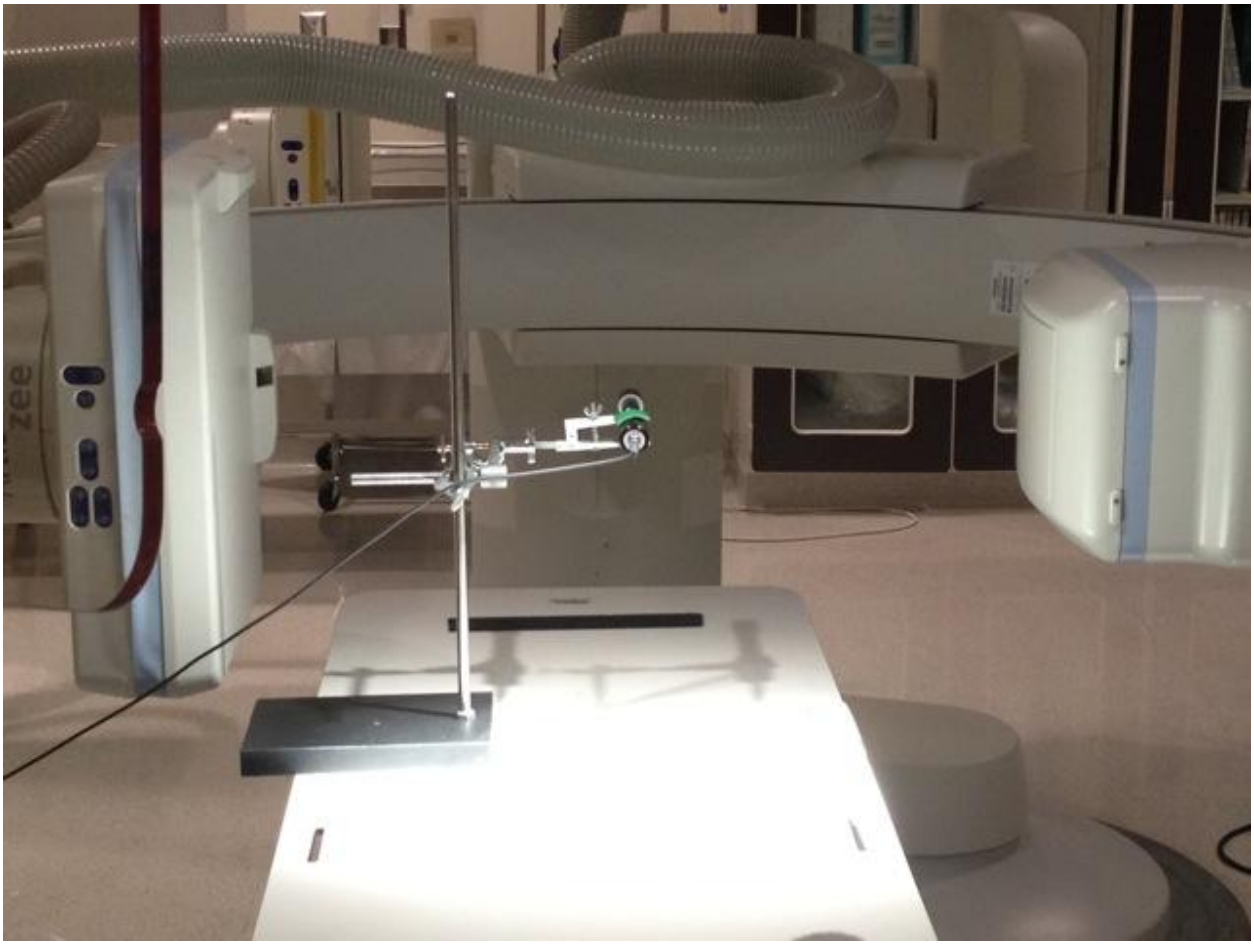

Figure 2-2. Calibration set up of KAP meter for the Siemens Artis Zee system. (Photo courtesy of David Borrego).

Table 2-1. Properties of the KAP meter installed in the Siemens Artis Zee system.

DIAMENTOR M4-KDK		
Measuring Range	DAP [μGym$^{2]}$	0.1-999,999
	DAP rate [μGym^2/s]	0.1-30,000
	Dose [mGy]	0.01-10000
	Dose rate [mGy/s]	0.01-999,999
	Irradiation time [s]	1s-999min
Digital Resolution	DAP [μGym$^{2]}$	0.01
	DAP rate [μGym^2/s]	0.01
	Dose [mGy]	0.001
	Dose rate [mGy/s]	0.001
	Irradiation time	600 ms (Dose rate>2.4μGy/s) 60ms (Dose rate>12μGy/s)
Ranges of Use	DAP rate	0.005-30,000 μGym^2/s
	Tube voltage	50-100 kVp
	Temperature	10-40^{o}C

Table 2-2. Radcal chamber 10x6-6 used for the DIAMENTOR meter calibration in the Siemens Artis Zee fluoroscopic unit. Chamber was last calibrated on 18-Sep-2012.

Chamber 10x6-6		
Min Rate	2 µR/s	20 nGy/s
Max Rate	17 R/s	149 mGy/s
Min Dose	10 µR	100 nGy
Max Dose	59 kR	516 Gy
Calibration Accuracy	±4% at 60 kVp and 2.8 mm Al HVL	
Exposure Rate Dependence	±5%, 0.4mR/s to 80 R/s, up to 500 R/s for 50 µs pulses	
Energy Dependence	±5%, 30 keV to 1.33 MeV	
Construction	Polycarbonate walls and electrode conductive graphite interior coating; 6.0 cm^3 active volume	

Table 2-3. Summary of irradiation settings for calibration of DIAMENTOR meter.

Filtration Material	Filtration Thickness (mm)	Tube Voltage (kVp)	Tube Current (mA)	Pulse width (ms)	Focal spot size
None	N/A	40, 50, 60, 70, 75, 80, 85, 90, 100, 110, 120	200	300	Small
Cu	0.1	40, 50, 60, 70, 75, 80, 85, 90, 100, 110, 120	100, 200, 300, 400, 500, 600	300, 600, 800, 1000	Small, Medium, Large
Cu	0.2	40, 50, 60, 70, 75, 80, 85, 90, 100, 110, 120	200	300	Small
Cu	0.3	40, 50, 60, 70, 75, 80, 85, 90, 100, 110, 120	100, 200, 300, 400, 500, 600	300, 600, 800, 1000	Small, Medium, Large
Cu	0.6	40, 50, 60, 70, 75, 80, 85, 90, 100, 110, 120	500	600	Small
Cu	0.9	40, 50, 60, 70, 75, 80, 85, 90, 100, 110, 120	500	600	Small

Table 2-4. Summary of the ten RDSR cases used for the testing of skin dose mapping software.

RDSR	Procedure	Age	Sex	Height (cm)	Weight (Kg)	Patient-Dependant Phantom	Cumulative $K_{a,r}$ (mGy)
1106	Endovascular stent graft repair of abdominal aortic aneurysm	72	M	177.8	117.9	[180cm/120kg]	8475.86
1193	Superior mesenteric artery stent placement	62	M	170.2	72.6	[170cm/75kg]	8406.56
1124	Bilateral uterine artery embolization	35	F	157.5	70.8	[160cm/70kg]	8191.52
1025	AAA stent graft repair	76	M	175.3	113.4	[175cm/115kg]	7581.00
1141	Cecostom tube replacement	24	M	134.6	59.0	[135cm/60kg]	6464.27
1325	Abdominal angiography; angioplasty of the superior mesenteric artery; stenting of celiac artery origin and bilateral renal arteries	63	M	175.3	73.5	[175cm/75kg]	6375.54
1166	Selective angiograph of celiac and superior mesenteric artery	81	M	175.3	89.8	[175cm/90kg]	6300.49
1150	Endovascular stent graft repair of abdominal aortic aneurysm	79	M	182.9	72.6	[180cm/75kg]	5856.81
1313	TIPS placement from right hepatic vein to right portal vein	50	F	165.1	72.6	[165cm/75kg]	5818.54
1322	Diagnostic arteriography of the lower abdomen/pelvis; embolization of left internal iliac artery and inferior mesenteric artery	19	M	177.8	71.2	[175cm/70kg]	5273.03

CHAPTER 3
RESULTS AND DISCUSSION

Calibration Coefficients

Figure 3-1 shows the reproducibility of measurements taken by the reference chamber and KAP meter. Both ionization chambers were exposed to 200 mA for 300 ms pulses with 0.1mm of copper filtration. These measurements were taken over a period of three months during which the KAP meter drifted by no more than 3%. The Radcal chamber measurements were within 2%. The small amount of variation in the measurements is surprisingly low given the uncertainties introduced by set up and determination of radiation field size. These results are advantageous for the adoption of calibration coefficients by demonstrating that the installed KAP while lacking accuracy is still precise.

Measurements covering a wide range of parameters for 0.1 and 0.3 mm of copper where made to help design the calibration procedure. Figure 3-2 shows how the calibration factor relates to the tube current and tube voltage. The beam filtration and tube current are statistically significant in the determination of the calibration factor while the tube current is not. No effects of saturation of either chamber were seen at high currents and voltages, in fact heat issues with the anode were the limiting factor in achieving higher outputs from the unit. These results indicate that only the tube voltage need be varied at each filtration to understand the behavior of the KAP meter.

Figure 3-3 shows the measured KAP values from the installed meter for 0.0 mm of copper filtration. A change in tube current yields a proportionate increase in the KAP value and no signs of saturation are evident at higher outputs. Figure 3-4 is the analogous version for the reference chamber. To calculate the calibration factors for 0.0

mm of copper filtration regression lines were fitted to the data and the quotient of them yielded the calibration factors seen in Figure 3-5. This figure illustrates that calibration factors can be described knowing only the tube voltage and inherent filtration of the incoming beam. This procedure was repeated for all filtrations to derive calibration coefficient curves. Figure 3-6, plots the calibration coefficients for all possible filtrations. For beams filtered with 3 mm or less of copper the calibration coefficient is monotonically decreasing. For harder beams, as seen with 0.6 mm and 0.9 mm, the behavior of the calibration coefficient is reversed which is consistent with previous studies.[11-13] In either case, the calibration coefficient is always less than unity indicating that the reported KAP and $K_{a,r}$ are overestimating dose to the patient.

Skin Dose Software

The skin dose mapping software was updated to include the calibration coefficients. Figure 3-7 (a) has mapped the skin dose on a patient-dependant hybrid phantom for a male undergoing a selective angiograph of the celiac and superior mesenteric artery. Before applying the correction factors this patient has a higher calculated peak skin dose than the cumulative reference air kerma; however, after taking into account the uncertainty in the KAP meter the peak skin dose drops by about 25%, Table 4-1. Figure 3-7 (b) shows the skin dose map after correcting for the KAP meter. Though rare, two effects contributed to the high peak skin dose. This procedure was static and not much panning was performed allowing for the dose to be concentrated on one spot. Secondly, the IEC defines the reference air kerma at a location 15 cm from the isocenter; therefore, if the patient's outer body contour lies beyond this point on the side closest to the tube the calculated dose will be higher than the registered reference air kerma. Relying only on the reference air kerma fails to

provide a good peak skin dose estimate or a spatial distribution of the dose. Both of these shortcomings are addressed in the skin dose mapping software and are further illustrated in Figure 3-8. This figure shows both the corrected and uncorrected peak skin dose plotted against the cumulative reference air-kerma provided by the RDSR along with a linear fit that corresponds to a one-to-one relationship between cumulative reference air-kerma and peak skin dose. This figure suggests that there is no correlation between these data.

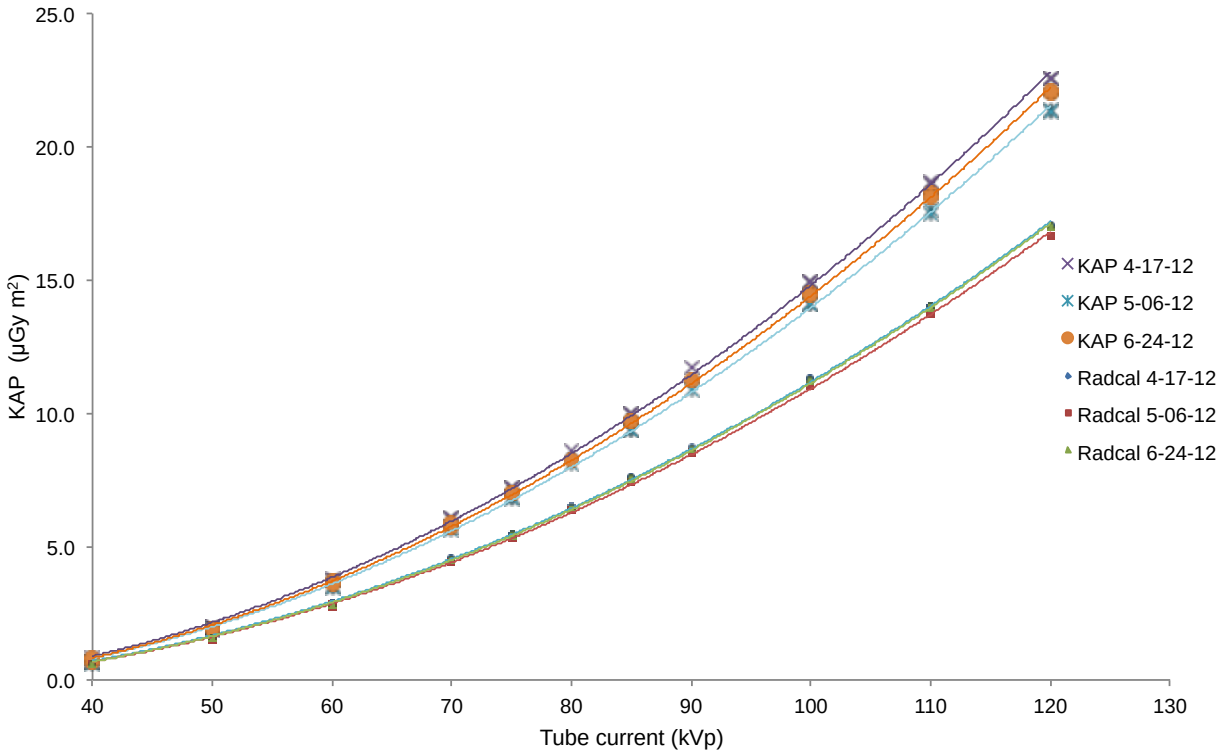

Figure 3-1. Measurements of KAP for the installed DIAMENTOR meter and reference chamber taken at a tube current of 200 mA and pulse width of 300 ms with 0.1 mm of copper filtration over a period of three months.

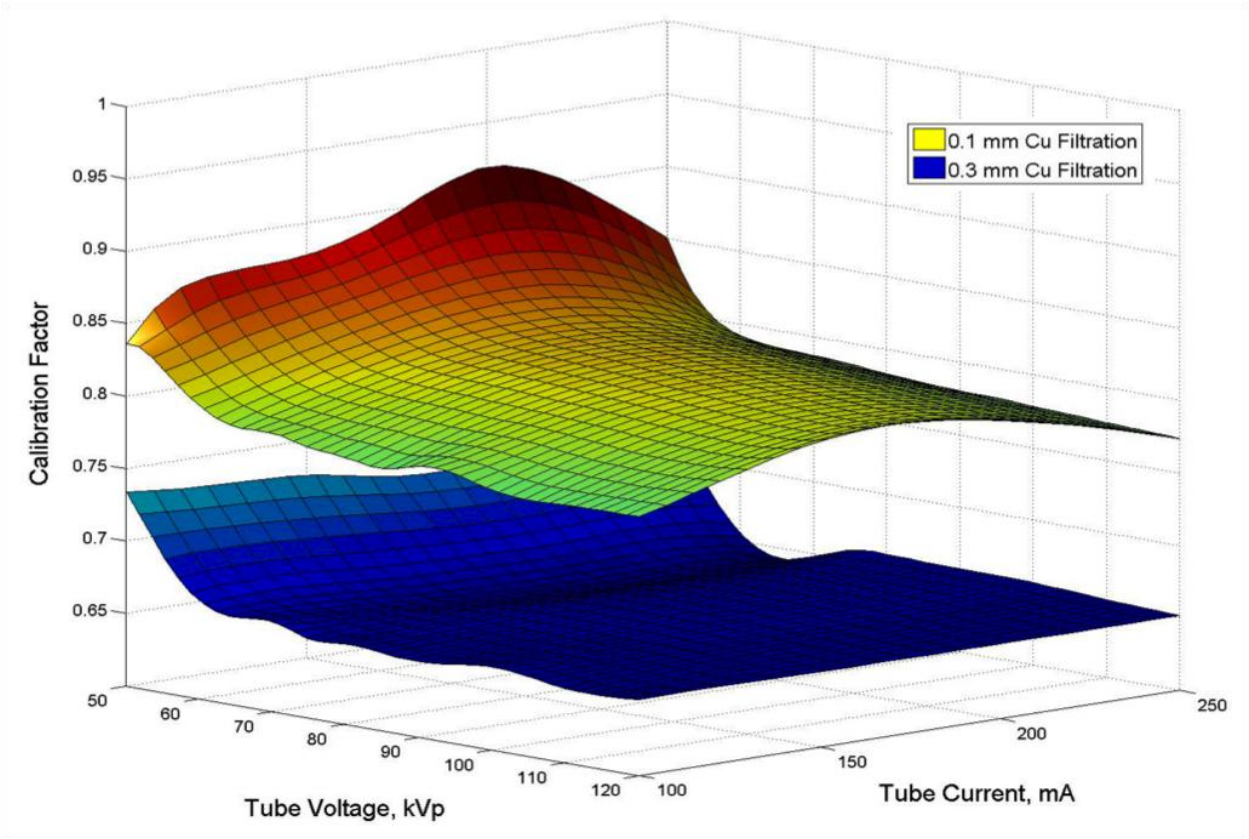

Figure 3-2. A best-fit plane over measured calibration factors for two different beam filtrations over a range of tube currents and voltages. Only the tube voltage and filtration influence the calibration factor.

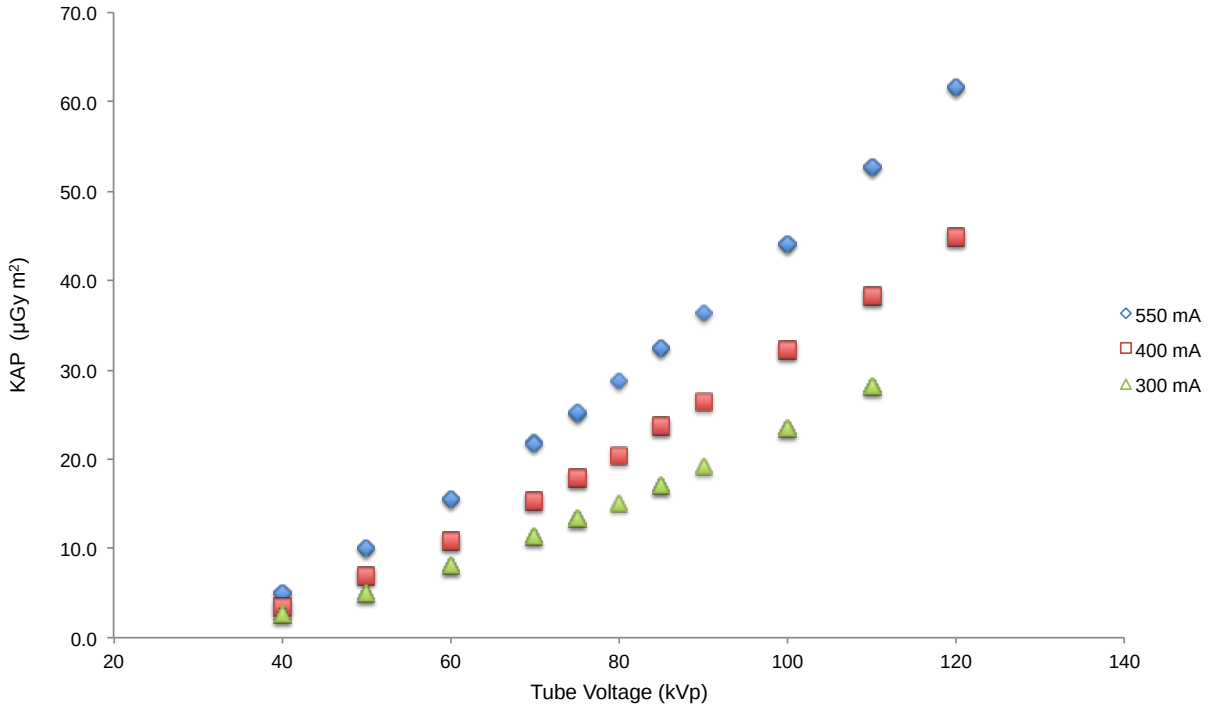

Figure 3-3. KAP readings corresponding to the DIAMENTOR installed in the Siemens Artis Zee system with no filtration.

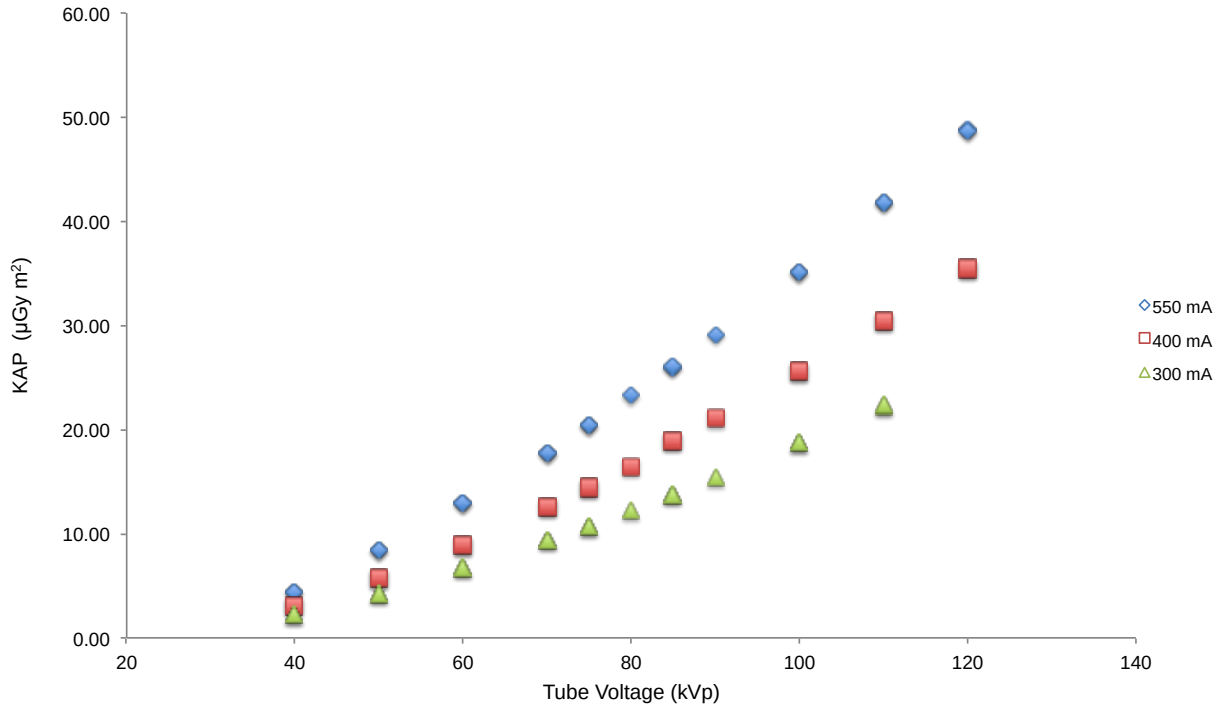

Figure 3-4. KAP readings made by the reference chamber at isocenter for the given radiation qualities with no beam filtration.

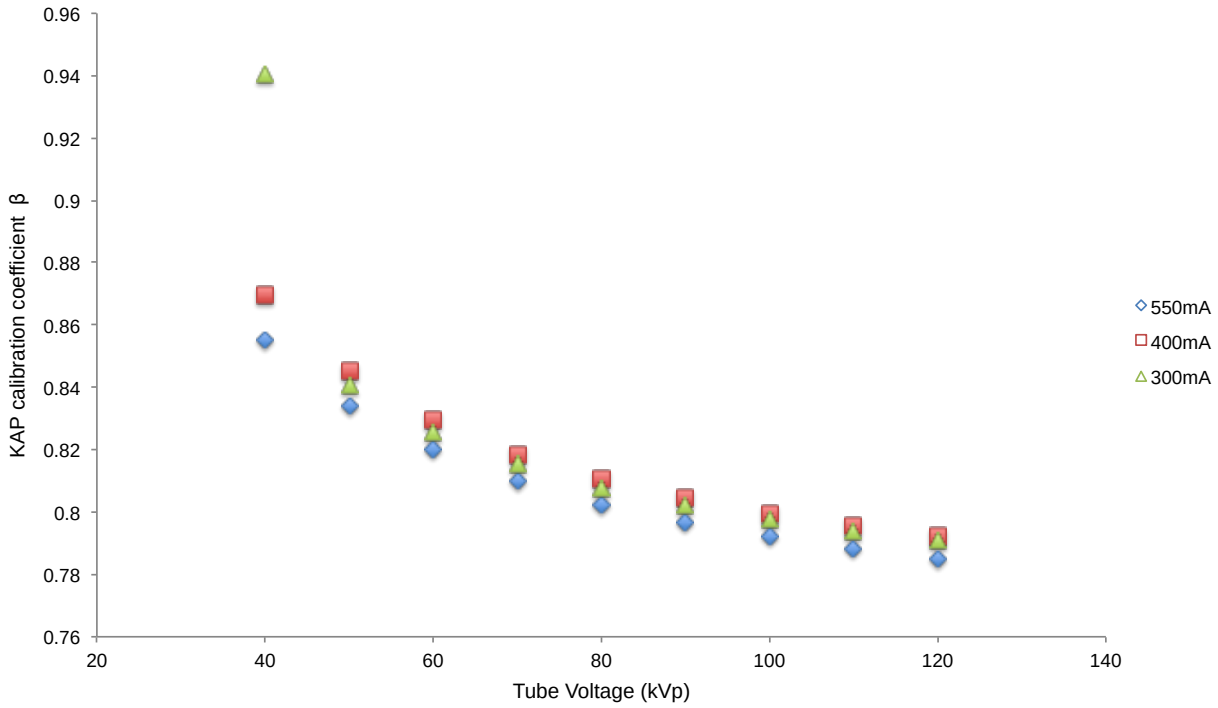

Figure 3-5. Calculated calibration coefficients with no tube filtration for the installed DIAMENTOR.

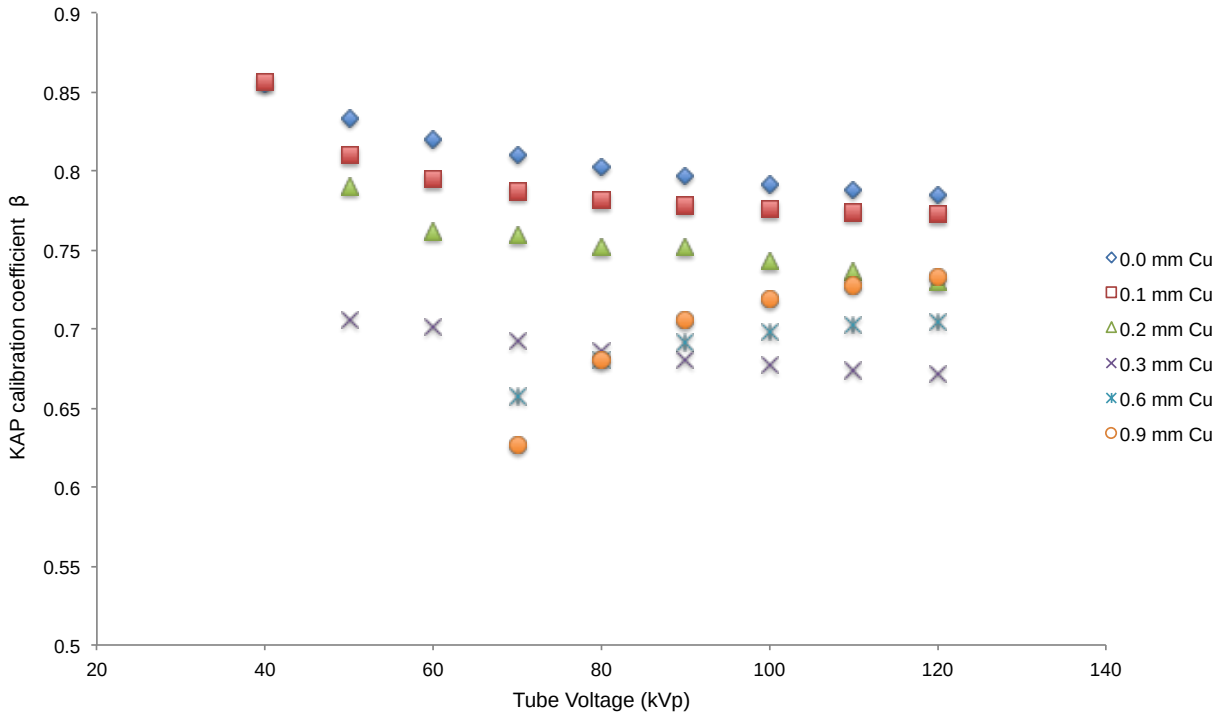

Figure 3-6. Calibration coefficients for each tube filtration available to the Siemens Artis Zee system.

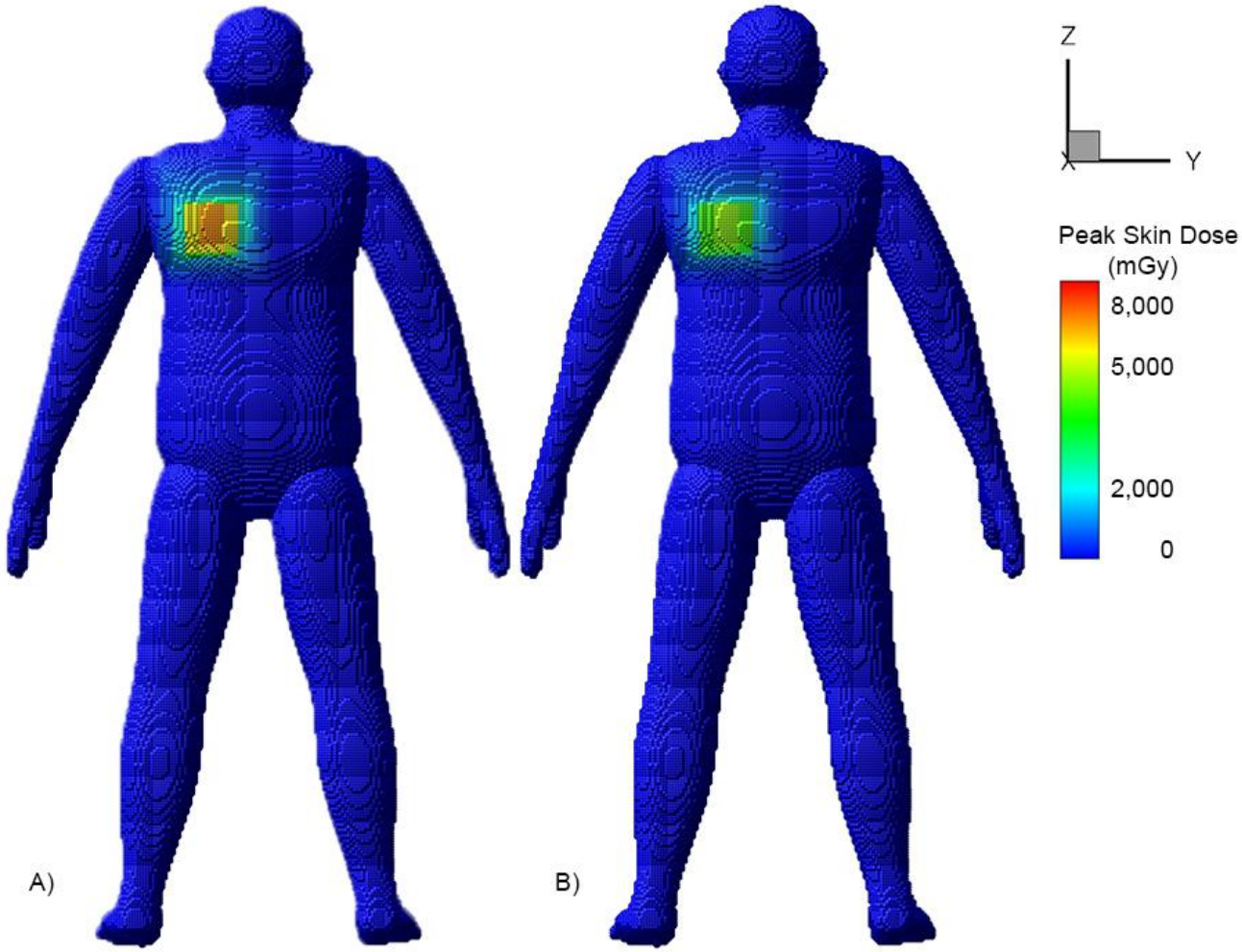

Figure 3-7. Results from the skin dose mapping software before (A) and after (B) applying the calibration coefficients for the KAP meter for a patient undergoing a selective angiograph of celiac and superior mesenteric artery.

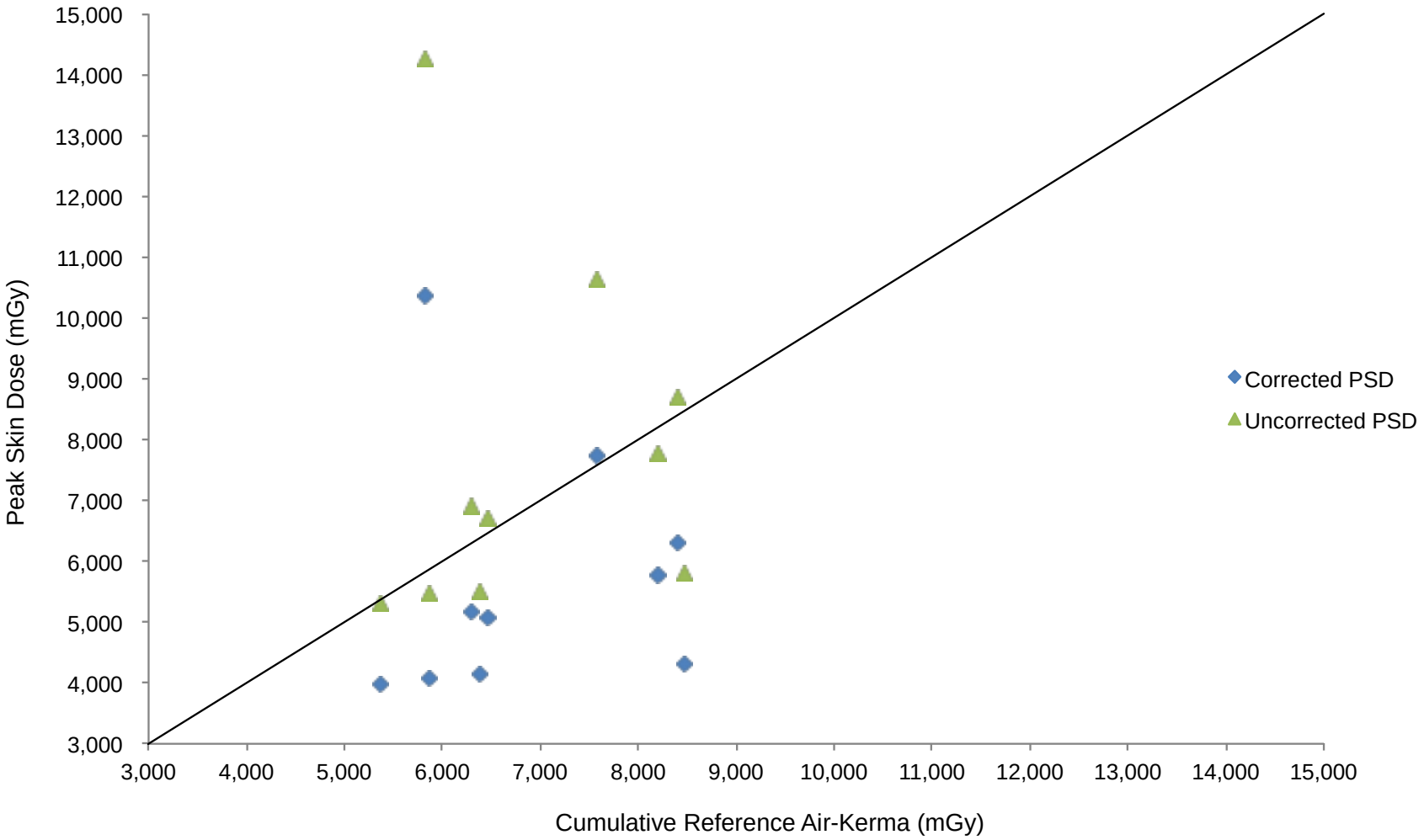

Figure 3-8. A comparison of peak skin doses from the skin dose software against cumulative reference air-kerma values obtained directly from the RDSR of the ten select patients.

Table 3-1. Results of the skin dose mapping software for a select group of high dose interventional fluoroscopic procedures.

RDSR	Procedure	Sex	Patient-Dependant Phantom	Cumulative $k_{a,r}$ Dose (mGy)	Peak Skin Dose w/o Calibration (mGy)	Peak Skin Dose w/ Calibration (mGy)
1106	Endovascular stent graft repair of abdominal aortic aneurysm	M	[180cm/120kg]	8476	5788	4292
1193	Superior mesenteric artery stent placement	M	[170cm/75kg]	8407	8704	6301
1124	Bilateral uterine artery embolization	F	[160cm/70kg]	8192	7773	5770
1025	AAA stent graft repair	M	[175cm/115kg]	7581	10631	7718
1141	Cecostom tube replacement	M	[135cm/60kg]	6464	6700	5072
1325	Abdominal angiography; angioplasty of the superior mesenteric artery; stenting of celiac artery origin and bilateral renal arteries	M	[175cm/75kg]	6376	5517	4134
1166	Selective angiograph of celiac and superior mesenteric artery	M	[175cm/90kg]	6300	6904	5163
1150	Endovascular stent graft repair of abdominal aortic aneurysm	M	[180cm/75kg]	5857	5457	4087
1313	TIPS placement from right hepatic vein to right portal vein	F	[165cm/75kg]	5819	14243	10359
1322	Diagnostic arteriography of the lower abdomen/pelvis; embolization of left internal iliac artery and inferior mesenteric artery	M	[175cm/70kg]	5273	5300	3971

CHAPTER 4
CONCLUSION AND FUTURE WORK

This study shows that it is possible to generate calibration coefficients for the KAP meter through in-clinic testing of its performance. The calibration coefficients are dependant only on the tube voltage and amount of filtration. Both of these parameters are contained in the RDSR for each irradiation event. The skin dose mapping software is then able to cull these variables, calculate the calibration coefficient, and finally apply the corrections in its calculation of peak skin dose.

This study is a small step in testing the hypothesis that in-procedure mapping of local skin doses, and post procedure documentation of internal organ doses, received by patients undergoing fluoroscopically guided interventions are clinically feasible and can take into account individual variation in patient body morphometry and dynamic nature of these procedures. Future work will put the skin dose mapping software through rigorous physical validation of its results and prepare it for clinical trials within the next two years.

LIST OF REFERENCES

1. J.R. Duncan, S. Balter, G.J. Becker, J. Brady, J.A. Brink, D. Bulas, M.B. Chatfield, S. Choi, B.L. Connolly, R.G. Dixon, J.E. Gray, S.T. Kee, D.L. Miller, D.W. Robinson, M.J. Sands, D.A. Schauer, J.R. Steele, M. Street, R.H. Thornton, R.A. Wise, "Optimizing radiation use during fluoroscopic procedures: proceedings from a multidisciplinary consensus panel," J. Vasc. Interv. Radiol. **22**, 425-429 (2011).

2. NCRP, "Ionizing radiation exposure of the population of the United States," National Council on Radiation Protection and Measurement, NCRP **Report No. 160** (2009).

3. FDA, "Initiative to reduce unnecessary radiation exposure from medical imaging," Center for Devices and Radiological Health, US Food and Drug Administration (2010).

4. NCRP, "Radiation dose management for fluoroscopically guided interventional medical procedures," National Council on Radiation Protection and Measurement, NCRP **Report No. 168** (2010).

5. S. Balter, J.W. Hopewell, D.L. Miller, L.K. Wagner, M.J. Zelefsky, "Fluoroscopically guided interventional procedures: a review of radiation effects on patients' skin and hair," Radiology **254**, 326-341 (2010).

6. P.B. Johnson, D. Borrego, S. Balter, K. Johnson, D. Siragusa, W.E. Bolch, "Skin dose mapping for fluoroscopically guided interventions," Med. Phys. **38**, 5490-5499 (2011).

7. The Joint Commission, "Sentinel event policies and procedures," (2012).

8. S. Balter, "Methods for measuring fluoroscopic skin dose," Pediatr. Radiol. **36 Suppl 2**, 136-140 (2006).

9. K. Chida, H. Saito, H. Otani, M. Kohzuki, S. Takahashi, S. Yamada, K. Shirato, M. Zuguchi, "Relationship between fluoroscopic time, dose-area product, body weight, and maximum radiation skin dose in cardiac interventional procedures," AJR Am. J. Roentgenol. **186**, 774-778 (2006).

10. P.B. Johnson, A. Geyer, D. Borrego, K. Ficarrotta, K. Johnson, W.E. Bolch, "The impact of anthropometric patient-phantom matching on organ dose: a hybrid phantom study for fluoroscopy guided interventions," Med. Phys. **38**, 1008-1017 (2011).

11. P. Toroi, T. Komppa, A. Kosunen, "A tandem calibration method for kerma-area product meters," Phys. Med. Biol. **53**, 4941-4958 (2008).

12. P. Toroi, T. Komppa, "Effects of radiation quality on the calibration of kerma-area product meters in x-ray beams," Phys. Med. Biol. **53**, 5207-5221 (2008).

13. P. Toroi, T. Komppa, "The energy dependence of the response of a patient dose calibrator," Phys. Med. Biol. **54**, N151-6 (2009).

BIOGRAPHICAL SKETCH

David Borrego was born to Adolfo and Martha Borrego in Las Vegas, NV. Shortly thereafter, David and his family moved to Medellin, Colombia where he would spend the next nine years of his life. David would not return back to the United States until the mid 1990's. His education in the United States started at the junior high level in Sewickley, PA. From an early age David took an interest in the natural sciences and mathematics. This interest led David to pursue a Bachelor of Science in Nuclear Engineering from the University of Florida. Currently, David is on track for a doctoral degree in medical physics from the Department of Biomedical Engineering at the University of Florida.